

## The rate of inflow and mixing during deep-water renewal in a sill fjord

Lars Arneborg, Carina P. Erlandsson, Bengt Liljebladh, and Anders Stigebrandt

Göteborg University, Box 460, SE-405 30 Göteborg, Sweden

### Abstract

We obtained high-resolution data on a deep-water renewal in the basin of Gullmar Fjord, Sweden, using an autonomous profiling platform. In the middle of the fjord, where the platform is anchored, renewal starts with the passage of a gravity current front and continues with a steady thickening of the new, oxygen-rich, low-nitrate bottom layer and an associated lifting of the old, oxygen-depleted, high-nitrate bottom water. The basin continuously fills to sill level during a period of 10 d. At the mouth of the fjord, a three-layer structure develops. Renewal is driven by the density difference between the intermediate water inside and the new deep water outside the fjord. The volume flux is well predicted by a hydraulic exchange model in which the upper layer plays a passive role. Local upwelling and downwelling of the upper halocline cause fluctuating baroclinic currents during renewal, but these seem to have little influence on the average volume flux of new deep water. Entrainment rates are small, and the associated volume flux increase seems to be balanced by detrainment.

Some fundamental hydrodynamic processes in the ocean that are quite important but notoriously difficult to study are activated during exchange of basin water in fjord basins. Exchange occurs when the water above sill level outside the fjord is denser than the residing deep water. Being denser, new deep water descends along the bottom of the fjord basin, whereby old basin water is pushed away and lifted to higher levels. The flow of new deep water toward greater depths should form a gravity-driven turbulent bottom current that can cause mixing with adjacent water. If the mixing takes the form of entrainment, adjacent, old deep water is thoroughly mixed into the current, which modifies the properties of the intruding water. However, if mixing occurs just at the interface between new and old deep water, water of intermediate density will be created and detached from the current when reaching the depth where the ambient density becomes equal. This type of mixing will lead to a decrease in the flow of new deep water with depth. The dynamics of dense gravity currents are of great general interest because such currents are major components in the vertical advection–diffusion circulation in ocean basins of all sizes. However, there are only few detailed observations of dense gravity currents along sloping bottoms. The initial speed and height and (negative) buoyancy of the flow when entering the fjord together with the vertical stratification and bottom topography in the fjord (slope and width) should govern the dynamics of the gravity current. Other interesting properties are speed, height and width of the flow, and the rate of mixing with ambient fluid, which are dependent on each other and cannot generally be studied separately.

Speed and height of dense gravity currents have been observed in vertical cross sections in larger systems with more permanent currents. Walin (1981) reported extensive obser-

uations in a vertical cross section of the Bornholm Channel in the Baltic. The entrainment into such permanent currents has also been observed in a number of cases (e.g., Baringer and Price 1997; Özsoy et al. 2001). In systems with more intermittent inflows, entrainment rates have mainly been inferred from the closing of budgets (e.g., Edwards and Edlsten 1976; Stigebrandt 1987a; Kouts and Omstedt 1993) and modeling. An entrainment parameterization was developed and tested in a vertical circulation model in Stigebrandt (1987b). The influence of the rotation of the Earth and Ekman dynamics on the entrainment process and on cross-isobath flow were also discussed. This parameterization was later much used, in particular in models of the Baltic Sea. Various parameterizations are described and reviewed in Liungman et al. (2001).

In fjords with relatively wide and deep mouths, new basin water can be exchanged in the course of days or hours. In quite large basins, inflow of new deep water can be an almost continuous process. Density variations in coastal water cannot be predicted in advance because they are governed largely by weather conditions. This explains why ongoing renewal of basin water is so hard to observe. The frequency of basin water exchange in fjord basins depends both on the intensity of vertical diffusion, which determines the rate of density decrease of the basin water, and on the characteristics of density variations outside the fjord. This problem has been treated and modeled by, for example, Gade (1973) and Aure and Stigebrandt (1990).

Only a few publications describing observations taken during events of basin water exchange in fjords are known. In the reported cases, intense measurement programs were running when exchange occurred by chance. Helle (1978) presents current time series and hydrographic observations during basin water exchange in the Byfjord on the Norwegian west coast. Molvær (1980) describes observations of basin water exchange in the Frierfjord at the Norwegian Skagerrak coast. Liungman et al. (2001) describe observations of basin water exchange in the Byfjord on the Swedish Skagerrak coast. Because the basin mouths are relatively narrow and shallow, the exchange of deep water continues for 1 week or longer in these fjords. In all three fjords, some

### Acknowledgments

This work was performed as part of the EU project OARRE: EVK3-CT1999-00002. The Seatrap platform and the sensors were partly funded by the EU project and partly by the K&A Wallenberg foundation. The new research vessel, *Alice*, used during deployment and recovery of the Seatrap mooring is a donation from the K&A Wallenberg foundation.

main characteristics of water exchange could be observed indirectly—namely, the uplift of the old, less dense basin water. In the Swedish Byfjord, it was also possible to infer the rate of entrainment of old deep water into the inflowing new deep water that is supposed to take place in dense gravity currents, although direct measurements were not undertaken.

The rate of exchange of basin water should depend on a baroclinic transport capacity of the mouth. This is generally thought of as a two-layer exchange, in which upwelling outside the fjord leads to a two-layer hydraulic control with a deep inflow and a surface outflow. Fluctuating barotropic currents can influence the transport capacity (Armi and Farmer 1986), and strong barotropic currents can temporarily sweep away the baroclinic controls and thereby increase the transport capacity of the mouth (Stigebrandt 1977). In the case of strong stratification above sill level inside and outside a fjord, one can suspect that the above results are inadequate to describe the baroclinic transport capacity. If the stratification inside and outside the fjord are well described by a two-layer stratification with the interface located above sill level, then a slight increase of the bottom layer density outside the fjord will be sufficient to generate a deep-water renewal. In that case, the exchange flow in the entrance will be a three-layer rather than a two-layer flow. This situation seems to be relevant for the Gullmar Fjord on the Swedish west coast, and probably for many other fjords, and will be discussed further in this paper.

The aim of this paper is to elucidate some of the hydrodynamic processes occurring during exchange of basin water in the Gullmar Fjord. To this end, we use a set of observations obtained by an oscillating platform operating along a vertical guide line in the fjord during an event of basin water exchange. Measured time series of salinity, temperature, oxygen, turbidity, and nitrate with high resolution, vertically and in time from the deepest part of the fjord, allow us to closely follow changes associated with the deep-water renewal. The physical oceanography of the Gullmar Fjord has been described in recent papers focusing on general water exchange (Arneborg 2004), internal waves (Arneborg and Liljebadh, 2001), and diapycnic mixing (Arneborg et al. in press).

## Instrumentation

During 17 d in April 2002, the Seatramp platform (Ocean Origo) was deployed in the central basin of Gullmar Fjord at 110 m depth (Fig. 1). Seatramp is an autonomous profiling platform that adjusts its volume, and thereby its buoyancy, by pumping oil between an internal and an external bladder. In Gullmar Fjord, it was deployed on a guiding line, restricting horizontal movement, but allowing vertical profiling from the bottom up to 2 m below the surface. It carries a number of sensors and can be programmed to sample these in either profiling mode or break mode. In profiling mode, the sensors are sampled continuously while the platform rises from the bottom to the surface. In break mode, which was used in Gullmar Fjord, the platform stops at selected depths and samples the sensors.

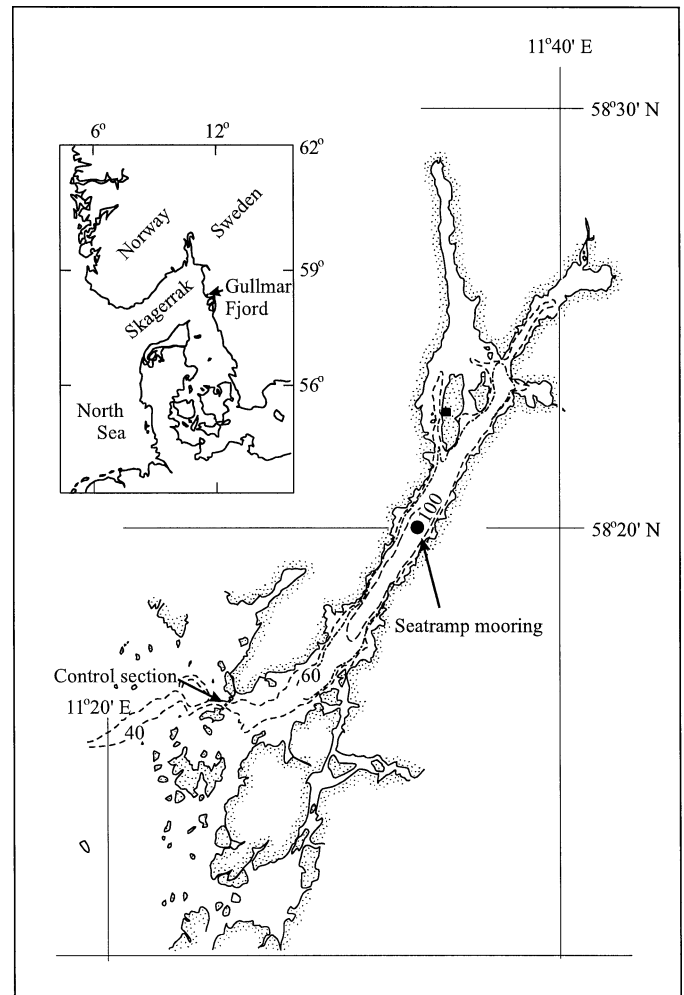


Fig. 1. Map of Gullmar Fjord showing the location of the Seatramp mooring and the control section in the main entrance.

The platform was equipped with a Seabird MicroCat conductivity-temperature-pressure (CTD) logger, an Oxyguard 505 oxygen sensor, a WS Ocean NAS-2E nitrate sensor, a Wetlab C-star transmissometer, and a Chelsea Instrument Minitracka II fluorometer. The oxygen sensor is a standard membrane-type sensor calibrated against humid air to 100% oxygen saturation before deployment. The nitrate sensor is an in situ autoanalyzer, reducing nitrate to nitrite in a cadmium column and measuring the concentration in water by conventional wet chemistry and colorimetric analysis techniques. The transmissometer measures the fraction of a red light beam (660 nm) that passes through a 25-cm water column. This has been calibrated against sediments from the deepest parts of Gullmar Fjord, giving the following relationship (Eq. 1) between the fraction of transmitted light, *Trans*, and sediment concentration, *c* (mg L<sup>-1</sup>).

$$c = -\frac{C \ln(\text{Trans})}{L_{\text{beam}}} \quad (1)$$

$C = 1.83 \text{ mg m L}^{-1}$  is a calibration constant and  $L_{\text{beam}} = 0.25 \text{ m}$  is the beam length. The fluorometer is an optical

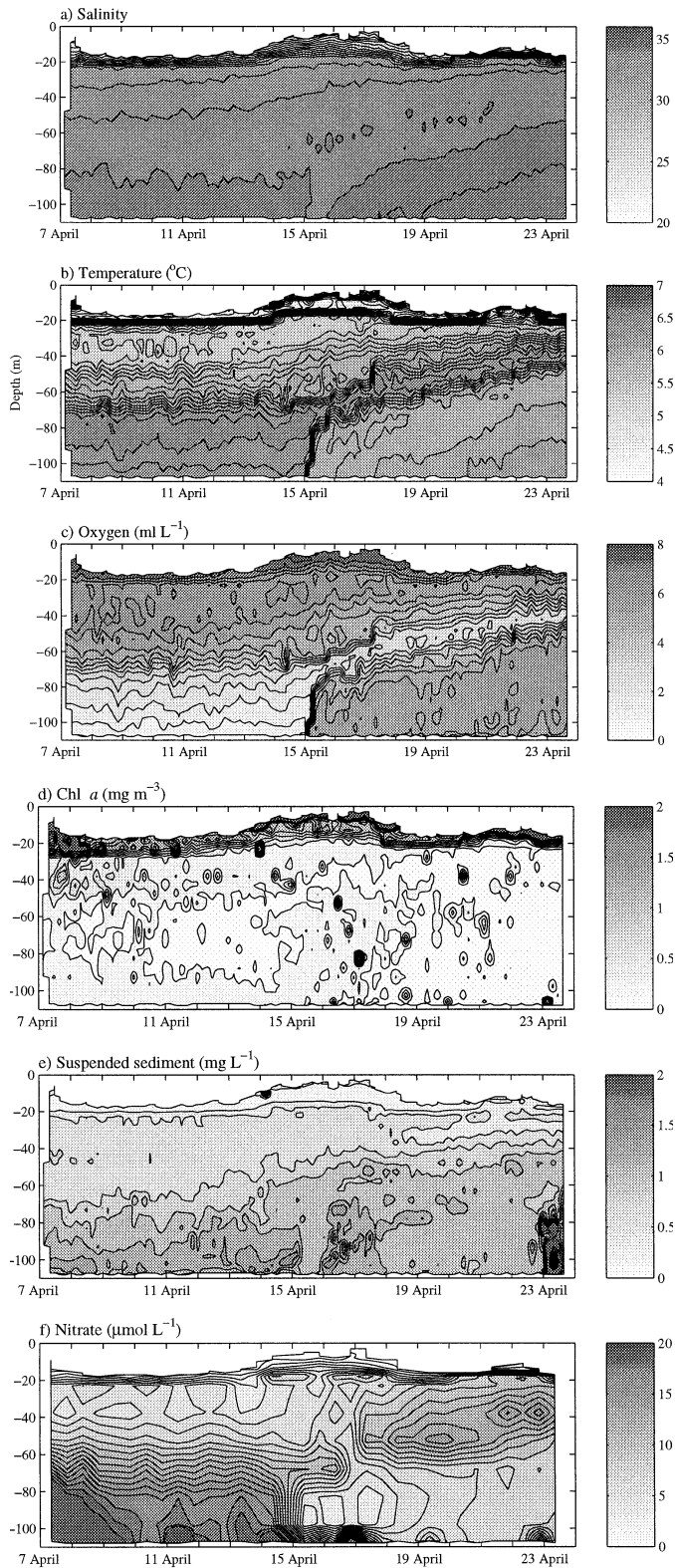


Fig. 2. Contour plots of (a) salinity, (b) temperature, (c) dissolved oxygen concentration, (d) chlorophyll *a*, (e) suspended sediment concentration, and (f) dissolved nitrate concentration.

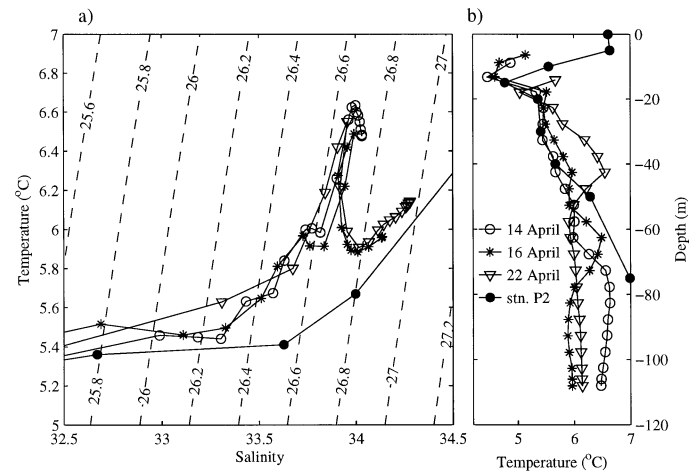


Fig. 3. (a) TS relations for vertical profiles on 14, 16, and 22 April. The curve marked with filled circles is a profile from station P2, 100 km south of the fjord on 15 April. The oblique lines are lines of constant density, and the density anomalies of these are indicated ( $\text{kg m}^{-3}$ ). (b) Temperature–depth relations for the same profiles as in panel a.

sensor that uses a single high-intensity blue light source and is calibrated by chlorophyll *a* dissolved in acetone.

The platform was programmed to profile from the bottom to the surface every fourth hour, stopping at 5-m intervals in the interior and decreasing the intervals near the bottom and surface. To ensure flushing of all instruments, the platform was set to wait for 2 minutes at each stop depth before sampling began. All instruments except the nitrate sensor sampled at all profiles and all stop depths. The nitrate sensor sampled only every third profile (i.e., two times a day) at selected stop depths because of limitations in analysis capacity of the sensor.

## Results

The results presented in this paper are from a deployment between 7 and 23 April 2002. Figure 2 shows the observations as functions of time and depth. The white areas at the surface are missing data, caused when the platform stopped before reaching the surface. Erroneous balancing caused the platform to stop at the  $1,016 \text{ kg m}^{-3}$  density surface rather than continuing to the surface. Temperature profiles from 14, 16, and 22 April are shown in Fig. 3b.

*Initial conditions*—The salinity plot (Fig. 2a) shows a halocline that separates the relatively homogeneous bottom water with salinities  $\sim 34$  from the surface water with salinities  $< 25$ . The halocline migrated vertically between 5 and 30 m depth. These movements were forced by similar movements of the halocline outside the fjord and are the main mechanism for the exchange of water above sill level (Arneborg 2004). The reason for these vertical movements outside the fjord have been discussed intensively in the past (Pettersson 1920; Shaffer and Djurfeldt 1983; Björk and Nordberg 2003). In the most recent publication (Björk and Nordberg

2003), the largest migrations were explained in terms of upwelling caused by local winds along the coast.

The temperatures initially had a local maximum of 6.6°C at 80 m depth, decreasing to 6.4°C at the bottom and 4.2°C in the coldest water in the halocline. The relatively warm water below 65–70 m depth was the stagnant bottom water residing there since the previous winter. The local temperature maximum was a memory from the previous summer/fall, when the bottom water was gradually heated by diapycnal mixing with the water above sill level, which was warmer at that time.

The dissolved oxygen concentrations decreased with depth from 8 ml L<sup>-1</sup> at the upper levels, which is almost 100% saturation, to 1 ml L<sup>-1</sup> at the bottom. The strongest decrease in rate was located at 60–70 m depth at the top of the stagnant bottom water. The low oxygen levels in the stagnant water were caused by remineralization of organic matter.

The chlorophyll levels were close to zero below the halocline and increased in the halocline. The chlorophyll levels were probably larger above the halocline, but we do not know this because the platform stopped at the top of the halocline. Local patches of relatively high chlorophyll levels appeared below the halocline, which might have been caused by falling organic matter.

The suspended sediment concentrations increased toward the bottom. This maximum must have been caused by re-suspension of sediments from the bottom because of the turbulent bottom boundary layer (Arneborg et al. in press). The maximum below the halocline was caused either by falling organic matter or by inflows of turbid water from outside the fjord.

The nitrate concentrations increased downward from ~5 μmol L<sup>-1</sup> at the surface to 18–20 μmol L<sup>-1</sup> at the bottom. The relatively high nitrate levels below sill level were caused by remineralization of organic matter since the previous deep-water renewal.

*Deep-water renewal*—On 15 April, an inflow that was dense enough to replace the residing bottom water occurred. Between 2310 h 14 April and 0310 h 15 April, a body of cold, oxygen-rich, nitrate-depleted water replaced the water up to 6 m from the bottom. Even the water 11 m from the bottom was slightly mixed with new water. Four hours later, the new water was present up to 26 m from the bottom, and 17 h later, at 1955 h 15 April, it was present at 73 m depth, 36 m from the bottom. After that, the increase in thickness of the new layer slowed down and turned into a slight decrease until the end of 16 April, when the increase in thickness started again at a slower rate than the first day. On 23 April, at the end of the data set, the new water occupied the basin up to about 50 m depth.

The warm, oxygen-deficient, nitrate-rich old water was replaced upward as the new water flowed in below (Fig. 2). The nitrate sensor did not sample at all depths and during all profiles; therefore, the picture is not as clear as for oxygen and temperature.

Another interesting feature is the lower initial salinity of the new water than the old bottom water. Nevertheless, the new water was slightly denser than the old water because of

the lower temperatures. Figure 3a shows the temperature–salinity (TS) relations from 14 April (the day before the renewal), 16 April (the day after the start of the inflow), and 22 April. The corresponding temperature–depth profiles are shown in Fig. 3b. The relatively warm, old bottom water is represented by the cluster of points with temperature 6.5°C and salinity 34. The new bottom water that entered the fjord was slightly less saline but colder (5.9°C) than the old bottom water, but gradually, the temperature and salinity of the new water increased with depth and time. The old water was seen as a warm, intermediate layer on 16 and 22 April. On 22 April, the density was almost 1,027 kg m<sup>-3</sup> at the bottom, which is 0.27 kg m<sup>-3</sup> denser than just before the inflow.

## Discussion

The main questions we want to answer with the data set are (1) what is the volume flux of the inflow, (2) what controls the inflow, (3) what is the height and width of the gravity current, and (4) how much is the volume flux of the new deep water modified by entrainment or detrainment before it reaches the fjord basin. We will end the section with a discussion about the local and regional conditions that cause a deep-water renewal.

*Volume fluxes*—The volume of the new water can be approximated as

$$V_{\text{new}} = \int_{-H}^{z_u} A(z) dz \quad (2)$$

where  $z_u$  is the upper boundary of the new water,  $H$  is the basin depth, and  $A$  is the hypsographic function. This is not completely correct because the upper surface of the new waterbody is not horizontal, but it gives a rough estimate of the volume changes. The volume of the new water, defined as the water with oxygen concentration >3.5 ml L<sup>-1</sup> and density >1,026.7 kg m<sup>-3</sup>, is shown as a function of time in Fig. 4. In the same plot, the volume of the old water with oxygen concentration <3.5 ml L<sup>-1</sup> is shown, and the volume below the upper halocline with salinity >28 is shown.

After the largest fluctuations during the first 2 d of the inflow, the volume of new water increased nearly linearly. The piecewise linear fit to the curve, shown in Fig. 4, corresponds to average volume fluxes of 1,300 m<sup>3</sup> s<sup>-1</sup> before 17 April and 600 m<sup>3</sup> s<sup>-1</sup> after 17 April.

The time when the new dense water enters the fjord can be estimated by calculating backward from the time when the nose of the gravity current passed the mooring. With a propagation speed of 0.08 m s<sup>-1</sup>, estimated below, and a distance of 12 km from the entrance to the mooring, one obtains the propagation time 42 h. This means that the water entered the fjord on 13 April in the morning. Between 13 and 24 April, the inflow of new water was (Fig. 4) 0.6 km<sup>3</sup>, which means that the average volume flux of new dense water through the entrance was 630 m<sup>3</sup> s<sup>-1</sup>.

The net inflow/outflow below the halocline and the associated outflow/inflow above the halocline can be found by inspection of the halocline movements. As seen in Fig. 2, the upper halocline migrated vertically with a period of

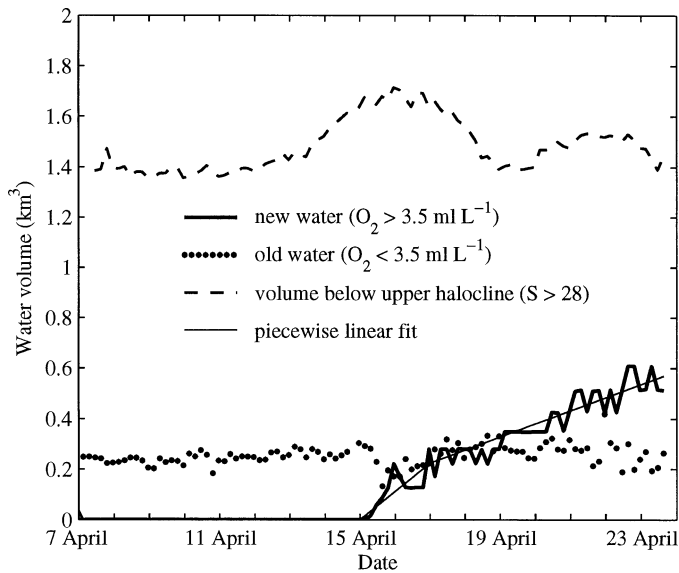


Fig. 4. Volume of new water ( $O_2 > 3.5 \text{ ml L}^{-1}$ ,  $\rho_\theta > 26.7 \text{ kg m}^{-3}$ ), volume of old water ( $O_2 < 3.5 \text{ ml L}^{-1}$ ), and volume of water below the upper halocline ( $S > 28$ ). Also shown is a piecewise linear fit to the new water volume.

about 7 d. This was much longer than the main internal seiche periods (1–3 d, Arneborg and Liljebadh 2001); therefore, the halocline could be taken as horizontal. The vertical halocline fluctuations were associated with large volume changes above and below the halocline and thereby with large baroclinic currents through the fjord entrance. This method to estimate baroclinic volume fluxes through the entrance has been validated against Acoustic Doppler Current Profiler (ADCP) measurements in the entrance in Arneborg (in press). The volume below the halocline is shown in Fig. 4. It is seen that  $0.3 \text{ km}^3$  was flushed into the fjord below the halocline between 12 and 16 April, while the same volume was flushed out from the upper layer (the sea surface movements were much smaller than the halocline movements). Between 16 and 19 April, the opposite exchange took place, with  $0.3 \text{ km}^3$  being flushed out of the fjord below the halocline and the same volume being sucked into the upper layer. Converted to volume fluxes, this means that the average volume flux into the fjord below the halocline between 12 and 16 April was  $870 \text{ m}^3 \text{ s}^{-1}$ . The maximum volume flux into the fjord happened between 13 and 15 April, with a magnitude of about  $1,100 \text{ m}^3 \text{ s}^{-1}$ . Between 16 and 19 April, the average volume flux out of the fjord below the halocline was  $1,100 \text{ m}^3 \text{ s}^{-1}$ .

The maximum inflow below the halocline ( $1,100 \text{ m}^3 \text{ s}^{-1}$ ) was somewhat smaller than the maximum rate of increase of new water in the deep basin ( $1,300 \text{ m}^3 \text{ s}^{-1}$ ). That the latter figure was larger can be explained either by outflow of old deep water below the halocline or by entrainment into the new water on its way from the entrance to the deep basin. Both of these effects are discussed below.

*Control of the rate of inflow*—In our analysis of flow control, we expected that the flow could be described by a three-layer model, the three layers being the upper layer above the

halocline, the resident water above sill level inside the fjord, and the new dense water entering the fjord. In addition, we made the following assumptions.

1. If there is a hydraulic control, then it is situated at the constriction between Flatholmen and Stångehuvud (Fig. 1) because the narrowest section with full sill depth occurs there. The actual sill is located in the archipelago outside this section. Current measurements at Flatholmen have shown that the major part of the water exchanges to the fjord flow through this section (Arneborg 2004).
2. The control section is approximated by a rectangular opening with width  $W_m = 350 \text{ m}$  and depth  $H_m = 43 \text{ m}$ .
3. The barotropic currents are small relative to the baroclinic currents. The argument for this is that the semidiurnal tides are weak ( $\sim 0.1 \text{ m}$  amplitude) and that low-frequency fluctuations in surface elevation ( $< 1 \text{ m}$ ) are much smaller than the low-frequency halocline fluctuations (5–15 m amplitude). Current measurements at Flatholmen (e.g., Arneborg 2004) support this assumption.
4. For small pressure differences in the upper layer, the upper layer flow is frictionally balanced rather than hydraulically controlled. This means that energy loss happens gradually on the way through the entrance, rather than in a hydraulic jump on the downstream side, and that the flow could be almost symmetric, rather than strongly asymmetric as is the case of a hydraulically controlled flow (e.g., Baines 1995). When the upper layer pressure difference, and thereby the velocities, become so large that information about (any) further pressure difference cannot pass freely through the entrance, the upper layer flow becomes hydraulically controlled.
5. The two lower layers are hydraulically controlled because of the strong asymmetry of the density field between the inside and the outside of the fjord.
6. As long as the upper layer is frictionally controlled, rather than hydraulically controlled, we expect that the upper interface can be approximated with a rigid lid. The argument for this approximation is that the density difference between the water above and below the halocline ( $\Delta\rho_1 \approx 10 \text{ kg m}^{-3}$ ) is much larger than the density difference between the lower layer of water inside and outside the fjord ( $\Delta\rho_2 = 0.3\text{--}0.5 \text{ kg m}^{-3}$ ).

We continue the analysis by assuming that the upper layer is frictionally balanced, and we will subsequently show that this must be valid. If the upper layer is frictionally balanced, then assumption 6 is relevant. In other words, the upper interface is a rigid lid, and the hydraulic exchange of the two lower layers cannot be distinguished from the exchange that would have occurred if the upper interface was the sea surface. Therefore, the theory for two-layer exchange with a net barotropic flow (Armi and Farmer 1986) can be applied directly. In our case, the net flow that influences the hydraulic two-layer exchange is

$$Q = Q_3 - Q_2 = -Q_1 \quad (3)$$

where  $Q_3$  is the inflow of dense water,  $Q_2$  is the outflow of intermediate fjord water, and  $Q_1$  is the inflow of upper layer water (Fig. 5). The last equality comes from the assumption of zero barotropic flow (assumption 3).

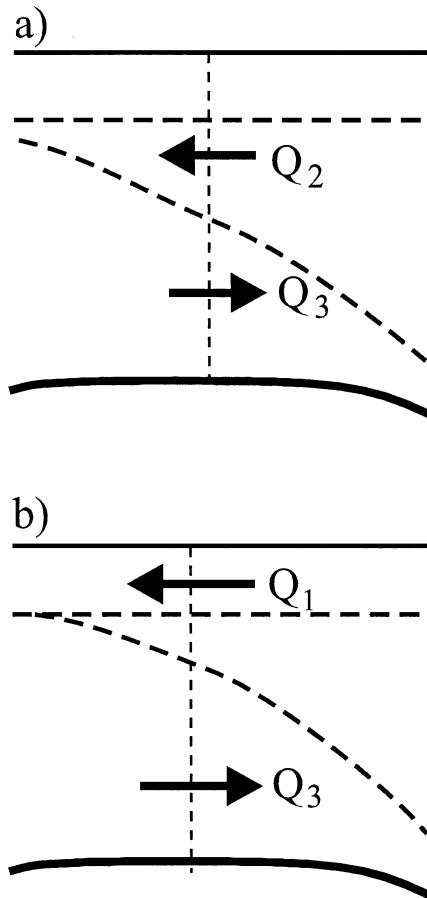


Fig. 5. Sketch of (a) maximum exchange with a stagnant upper layer and (b) deep-water inflow with a blocked outflow of intermediate fjord water.

In the special case (Fig. 5a) of no net flow in the two lower layers (or in the upper layer), the maximum exchange flow (Armi and Farmer 1986) obtained at the narrowest cross section in the entrance is

$$Q_{3a} = \frac{W_m}{4} [g'_2 (H_m - h_1)^3]^{1/2} \quad (4)$$

where  $g'_2$  is the reduced gravitational acceleration based on the density difference between the water inside and outside the fjord below the halocline,  $H_m$  is the sill depth, and  $W_m$  is the width of the mouth. In order for Eq. 4 to be valid, the upper surface of the new water outside the fjord must be above the midpoint between the sill and the upper halocline.

Another special case is that in which the inward net flow becomes so strong that the intermediate outflow is blocked (Fig. 5b). In that case, hydraulic control in the lower layer gives the volume flux (Eq. 5; Armi and Farmer 1986).

$$Q_{3b} = W_m \left\{ g'_2 \left[ \frac{2}{3} (H_m - h_1) \right]^3 \right\}^{1/2} \quad (5)$$

The same expression can be used for the outflow of intermediate fjord water when the inflow of dense water is blocked.

After inserting the relevant numbers for Gullmar Fjord—

$W_m = 350$  m,  $H_m = 43$  m,  $h_1 = 20$  m,  $g'_2 = 0.004$  m s<sup>-2</sup>—one obtains the exchange flows  $Q_{3a} = 610$  m<sup>3</sup> s<sup>-1</sup> in the case of no upper layer motion and  $Q_{3b} = 1,330$  m<sup>3</sup> s<sup>-1</sup> for the case of no intermediate layer outflow.

In the previous subsection, we found that the maximum volume fluxes in the upper layer were in the order of  $|Q_{1\max}| \approx 1,100$  m<sup>3</sup> s<sup>-1</sup>. This is less than is needed ( $Q_{3b}$ ) to block the intermediate fjord water outflow or deep-water inflow. This means that if the upper layer flow is frictionally balanced, then none of the two lower layers are blocked at any time during the measurements.

It remains to be shown that the upper layer must have been frictionally balanced (i.e., that it cannot have been hydraulically controlled). The strongest upper layer currents in the two cases described above occur in the limiting situation when the intermediate or bottom layers are blocked. If the upper layer is not hydraulically controlled during these situations, it is not probable that it is controlled at weaker current velocities either, so we assume that the intermediate layer is blocked. In order for the upper layer to be controlled, the upper layer volume flux must be described by Eq. 6.

$$Q_{1c} = -W_m \left[ g'_1 \left( \frac{2}{3} h_1 \right)^3 \right]^{1/2} \quad (6)$$

Inserting the same values as above and  $g'_1 = 0.1$  m s<sup>-2</sup>, one obtains  $Q_{1c} = -5,390$  m<sup>3</sup> s<sup>-1</sup>. This is a much stronger current than the value  $Q_{1b} = -1,330$  m<sup>3</sup> s<sup>-1</sup> found under the assumption of a frictionally balanced upper layer. It is also stronger than the maximum volume flux ( $-1,100$  m<sup>3</sup> s<sup>-1</sup>) calculated from halocline movements. In other words, the main assumption behind the calculation of  $Q_{1b}$  (that the upper layer is not hydraulically controlled) is valid. The upper layer current is not strong enough to cause hydraulic control in the upper layer.

The analyses above indicate that the following picture of the inflow is reasonable. The inflow of dense water began on 13 April in the morning. After the upper surface of the new water outside the fjord rose above the midpoint between the sill and the halocline, the inflow of dense water and outflow of intermediate fjord water developed into a maximum exchange flow below the upper halocline. The upper layer flow was a frictionally balanced subcritical flow. The maximum exchange flow was influenced by the net currents below the upper halocline, but these currents were never so strong that they blocked the exchange.

As an average over the whole period from 13 to 24 April, the budget calculations gave a volume flux of new water into the basin of 630 m<sup>3</sup> s<sup>-1</sup>. This compares well with the estimate  $Q_{3a} = 610$  m<sup>3</sup> s<sup>-1</sup>, calculated assuming maximum exchange in the lower layers and zero net flow above and below the upper halocline. These two values are, however, not directly comparable because the volume flux into the basin includes the effects of entrainment and detrainment between the entrance and the deep basin. These effects are discussed below.

*Height and speed of the gravity current at Alsbäck—* Along the sloping bottom inside the sill, the flow of new deep water should take the form of a gravity-forced dense

bottom current balanced by bottom friction. When the current reaches the greatest depth, the advection of new deep water further into the fjord should be forced by the density difference between old and new deep water. We thus expect that the flow of new deep water experiences two different dynamical regimes: the first, down the slope, and the second, further advection into the fjord. Below, we discuss these flow regimes.

The flow of the new dense deep water down the slope takes the form of a frictionally balanced gravity current. The mean slope  $s$  of the bottom from the entrance to the mooring is about 80/12,000, so  $s \approx 0.007$ . The slope, together with the density difference, provides the forcing of the flow against friction. We assume that frictional forces are proportional to speed squared with the proportionality factor (drag coefficient)  $C_D$  equal to about 0.003. The volume flow through the mouth is  $Q$ , and the buoyancy flux is  $B = Qg'$ , where  $g' = g\Delta\rho/\rho_0$ . The gravity current has the height  $h$ , speed  $u$ , and width  $W$ . Applying the model of a frictionally balanced gravity current in Stigebrandt (1987b), the speed and height of the gravity current is given by the following expressions.

$$u = \left( \frac{s}{C_D} g' h \right)^{1/2} \quad (7)$$

$$h = \left( \frac{C_D q^2}{s g'} \right)^{1/3} \quad (8)$$

Here,  $q = uh$  is the specific transport (per unit width). For slowly varying bottom slope, drag conditions, and ambient stratification,  $u$  and  $h$  adapt to the local values. To estimate  $u$  and  $h$ , we assume that there is no entrainment into the gravity current. From the rate of filling (*see above*), we find that  $Q \approx 1,300 \text{ m}^3 \text{ s}^{-1}$  during the first days of inflow. The local value of the density difference between the gravity current and the ambient water is  $\Delta\rho = 0.02 \text{ kg m}^{-3}$  at the bottom of the basin, and the local width of the current is assumed to be  $W = 500 \text{ m}$ . This gives  $q = 2.6 \text{ m}^2 \text{ s}^{-1}$ . Finally, insertion gives the speed  $u = 0.1 \text{ m s}^{-1}$  and the height  $h = 24 \text{ m}$ . If the drag coefficient is changed by a factor of two, the speed and height change by 20–25%.

Because the mean  $s$  is greater than  $C_D$ , the flow should be supercritical ( $u > [g'h]^{1/2}$ ) at least in some stretches along its route. Supercritical flows are often related to low Richardson numbers, which could lead to the generation of instabilities at the interface and mixing between the new and old deep water. The mixing can be estimated by the model in Stigebrandt (1987b), which we do in the following subsection.

When the front of the current reaches the bottom of the basin, it continues to propagate into the fjord because of the density difference. This is probably the relevant regime for the current as it reaches the mooring at Alsback. The results of laboratory experiments show (*see p. 103 in Baines 1995*) that gravity currents at high Reynolds numbers propagate at speeds

$$U = K(g'h)^{1/2} \quad (9)$$

where  $h$  is the height of the gravity current and  $K = O(1)$

is a function of the relative height of the gravity current. Equation 9 just expresses a balance between the acceleration of the water in front of the head and the pressure difference between the gravity current and the undisturbed water in front of the gravity current. With the same density difference as used in Eqs. 7 and 8 ( $\Delta\rho = 0.02 \text{ kg m}^{-3}$ ) and the observed gravity current height of about 30 m, one obtains a gravity current front velocity  $U = O(0.08 \text{ m s}^{-1})$ . The particle speed behind the front can be estimated by Eq. 10.

$$u = \frac{Q}{hW} \quad (10)$$

Inserting  $Q = 1,300 \text{ m}^3 \text{ s}^{-1}$ ,  $h = 30 \text{ m}$ , and  $W = 500 \text{ m}$ , one obtains  $u = 0.09 \text{ m s}^{-1}$ . The difference between  $u$  and  $U$  might indicate a loss of fluid at the gravity current head, but the uncertainties in  $Q$  and  $W$  are too large to make such conclusions.

If moving at speed  $U = 0.08 \text{ m s}^{-1}$ , the nose that passed the mooring around 0000 h 15 April will have moved 3.5 km further into the fjord at 1200 h 15 April, when the thickest part of the current passed the mooring. The length of the gravity current head was therefore about 100 times longer than the height. This is very different from laboratory gravity currents in which the height and length are of equal magnitude (Simpson 1987). Possible reasons for this difference are the irregular bottom topography, continuous rather than layered stratification, and bottom friction. The difference will have large consequences for mixing at the gravity current head and illustrates the need for observations of geophysical gravity currents.

*Entrainment and mixing*—In order to estimate the entrainment, we need to know the water properties outside the fjord. For this purpose, we have a profile from the monthly monitoring station P2 located about 100 km south of Gullmar Fjord. The profile is from 15 April (i.e., at the beginning of the inflow). Because of the lack of measurements closer to Gullmar Fjord, we will assume that the water masses at station P2 are representative of the water masses just outside the fjord.

The TS relationship (Fig. 3) from before the inflow ends in a cluster of relatively warm ( $\sim 6.5^\circ\text{C}$ ) and saline ( $\sim 34$ ) points. This was the deep water below 70 m depth. After the inflow, the old deep water was still present, but a new and colder branch representing the new deep water has been added to the TS curves. The new branch is situated between the coastal (station P2) water curve and the old water curve, which indicates that the new water is a mixture of old fjord water and coastal water as expected. The new branch in the TS curves has a temperature minimum of about  $5.9^\circ\text{C}$ . The water masses below (with higher density than) the temperature minimum are situated closer to the P2 curve than to the old water curve, which indicates that the new water mainly contains coastal water. By drawing a straight line from the cluster of old water points, through the temperature minimum water, and continuing through the P2 water, we find that the temperature minimum water contains about 25% old water and 75% coastal water. Similarly, we find that the densest new water contains about 17% old water and 83% coastal water. During the first day of the inflow,

before the old water below 70 m is lifted to sill level, the inflowing coastal water also comes into contact with the fjord water above 70 m. It therefore is a theoretical possibility that the temperature minimum water is a mixture between coastal water with density  $1,026.9 \text{ kg m}^{-3}$  and fjord water with density  $1,026.6 \text{ kg m}^{-3}$ . In that case, the new water contains about 40% old water and 60% coastal water. This must be seen as an absolute maximum content of old water, possible only for the water that enters the fjord during the first day if all the entrainment happens above 70 m depth.

A second way to estimate the amount of old water in the new basin water is to look at oxygen concentrations. The oxygen concentration in the relevant water at station P2 was about  $6.7 \text{ ml L}^{-1}$ . The old basin water below 70 m depth had oxygen concentrations ranging from 1 to  $4 \text{ ml L}^{-1}$ , with a volume average of about  $2.5 \text{ ml L}^{-1}$ . The oxygen concentration of the new water was about  $5.7 \text{ ml L}^{-1}$ , which indicates that it should contain  $\sim 76\%$  coastal water and 24% old water. This is in good agreement with the estimate from the TS diagram, which supports the assumption that P2 is representative of inflowing waters.

The results above, based on water properties, indicate that the volume flux of new water through the entrance increases  $\sim 33\%$  on the way downslope because of entrainment of old basin water. This is relatively little when compared with other overflows that have been studied, in which the initial volume flux typically increases by factors of two to four because of entrainment (e.g., Baringer and Price 1997; Liungman et al. 2001). Next, we investigate whether such small entrainment rates can be predicted with existing models.

It is common to define an entrainment coefficient,  $E$ , as in Eq. 11,

$$E = \frac{1}{u} \frac{dq}{dx} \quad (11)$$

where  $x$  is the along-channel coordinate. Various parameterizations of the entrainment coefficient are reviewed in Liungman et al. (2001). Stigebrandt (1987b) developed a model based on a Kato–Phillips-type entrainment parameterization, in which the turbulence that entrains the ambient fluid is generated by bottom shear stress. With his parameter choice, the parameterization is

$$E = 0.071s \quad (12)$$

where  $s$  is the bottom slope. This is similar to an empirical result of Pedersen (1980) that was based on observations of the Denmark Strait overflow. The same value for the bottom slope as used above, ( $s \approx 0.007$ ) gives the entrainment coefficient  $E \approx 5 \times 10^{-4}$ . The velocity can be calculated from Eqs. 7 and 8. The density difference between the inflowing and ambient waters decreases from  $\sim 0.4 \text{ kg m}^{-3}$  at sill level to  $0.02 \text{ kg m}^{-3}$  at the bottom of the basin. With a volume flux  $Q = 1,300 \text{ m}^3 \text{ s}^{-1}$ , these density differences give velocities in the range  $0.1\text{--}0.3 \text{ m s}^{-1}$ . Initially, the entrainment happens over a distance of 12 km, but as the upper interface of the new water rises, this distance quickly decreases. Within the first hours of the inflow, the interface rises to 80 m depth, which means that the entrainment distance decreases to 5–6 km. The values  $u = 0.2 \text{ m s}^{-1}$  and distance = 6 km

give the total increase in specific volume flux  $\Delta q = 0.6 \text{ m}^2 \text{ s}^{-1}$ . With a channel width of 500 m, the total volume flux increase by entrainment is  $Q_E = 300 \text{ m}^3 \text{ s}^{-1}$ , or 23% of the new water that reaches the deep basin ( $1,300 \text{ m}^3 \text{ s}^{-1}$ ). It is seen that this prediction, based on the Stigebrandt (1987b) bottom current model, fits well with the entrainment estimates that are based on water properties (24%). One important reason for the small amount of entrainment relative to what has been observed in other systems is the small density difference between the new and old waters. From Eq. 11, we get Eq. 13.

$$q^{-1} \frac{dq}{dx} = \frac{E}{h} \quad (13)$$

That is, the relative increase in volume flux is inversely proportional to the thickness. A small density difference gives a large thickness and, thereby, a small relative volume flux increase by entrainment.

Besides entrainment, symmetrical mixing at the interface could create water of intermediate density. Such mixing could lead to detrainment from the bottom current when the mixed fluid reaches the depth where the ambient density becomes equal, as discussed at the beginning of this paper. This would cause a relatively oxygen-rich layer of the same densities as the old water located above the gravity current close to the entrance. There were no signs at the mooring of increased oxygen levels in the intermediate layer of old water caused by intruding layers of high oxygen content. This does not rule out the possibility of detrainment because the oxygen-rich mixed layers can be concentrated at the entrance without spreading out into the interior of the fjord. If we assume that the isopycnals are reasonably horizontal outside the bottom current, such a water mass would be seen at the mooring as an apparent volume increase of the old and mixed water masses. On the contrary, entrainment into the bottom current would be seen as a decrease in volume of the old water masses, which is, however, relatively constant, as seen in Fig. 4. This indicates that the volume decrease of the old fjord water by entrainment is balanced by an increase by detrainment. Similarly, the volume increase of the inflowing new bottom water by entrainment seems to be balanced by a similar volume decrease by detrainment (i.e., the volume flux of the bottom current remains constant and the negative buoyancy flux decreases).

*Coastal forcing*—The results reported in “Control of the rate of inflow” show that deep-water inflow is caused by an increase in density of the deep water outside the fjord and that the inflow is relatively insensitive to local upwelling and downwelling of the layer above the halocline. But what causes the increase in the density of water above sill level but below the halocline?

Aure and Sætre (1981) showed that persistent winds with a component from the northeast induce outflow of surface water from Skagerrak, whereas winds with a southwesterly component tend to block outflow of low-saline surface water. This general behavior has been verified by a model of the wind-driven surface circulation in Skagerrak (Stigebrandt 1984) and by analyses of hydrographic data (Gustafsson and Stigebrandt 1996). Thus, persisting northeasterly winds over

Skagerrak remove low-saline surface water that is replaced by saltier and denser water welling up from greater depths. This explains the often noticed circumstance that exchange of deep water in the fjords along the Swedish west coast can occur when an atmospheric high pressure cell parks for a long time over northern Scandinavia. Thus, to explain vertical movements of density surfaces at the coasts of Skagerrak, one has to account for the large-scale circulation in Skagerrak and not only consider local effects of the wind. This is supported by results presented by Aure et al. (1997), who analyzed 1-yr-long time series obtained from several depths in a mooring at 100 m water depth off the Norwegian coast. They found that most of the variability of the density field was from horizontal advection along the coast of horizontal gradients by the large-scale circulation and that only relatively little could be explained as the result of local up- and downwelling from the action of the wind. They also found that about half of the variability was contained in the annual cycle, with maximum density in early spring. The latter was explained by Gustafsson and Stigebrandt (1996) as a result of northeasterly winds that often occur in early spring. However, a temperature minimum also occurs in early spring, which explains about half of the annual density cycle, as pointed out by Arneborg (in press).

The reason most deep-water renewal events in Gullmar Fjord happen in early spring, therefore, is a combination of the temperature minimum and the salinity maximum at depth. However, the more specific timing and strength of a renewal is solely governed by the regional winds and large-scale circulation of Skagerrak.

In conclusion, an inflow of dense, oxygen-rich, low-nitrate, turbid water to the deep basin of Gullmar Fjord, and the associated rising of the old oxygen-depleted, high-nitrate bottom water, was observed with an autonomous profiling platform. The observed part of the inflow lasted for 10 d and filled the basin to sill level with new water. The inflow began on 13 April 2002 and passed the mooring 12 km from the entrance on 15 April as a 30-m-high and 4-km-long gravity current traveling at a speed of about  $0.08 \text{ m s}^{-1}$ .

The average volume flux in the inflow was  $630 \text{ m}^3 \text{ s}^{-1}$ . This volume flux was well predicted by assuming maximum hydraulic exchange between the intermediate fjord water and the new bottom water outside the fjord. Fluctuating exchanges caused by movements of the upper halocline influenced the bottom–intermediate water exchange but did not block it and did not change the average exchange from that obtained by assuming a stagnant upper layer. This means that the renewal was forced by the difference in density of the intermediate water inside and outside the fjord and that the local, wind-driven upwelling/downwelling of the upper halocline was relatively unimportant.

Entrainment was estimated by comparing the water that reached the fjord basin with the water 100 km south of the fjord. If this water was representative of the water that entered the fjord, the water that reached the fjord basin contained about 75% coastal water and 25% old basin water that was entrained into the bottom current. The entrainment was relatively well predicted by an existing model. The estimated entrainment rates were much smaller than had been found in other overflows. The main reason for the small

entrainment rates was the small density difference between the new and old waters, which led to a thick gravity current.

The volume of the old water remained constant as it was lifted upward, in spite of the loss to entrainment into the bottom current. This indicated that entrainment was balanced by an equal amount of detrainment caused by symmetrical mixing at the interface between the bottom current and the old water.

A future study should concentrate on the bottom current itself by investigating the dynamics of the bottom current and obtaining better estimates of entrainment and detrainment processes.

## References

- ARMI, L., AND D. M. FARMER. 1986. Maximal two-layer exchange through a contraction with barotropic net flow. *J. Fluid Mech.* **164**: 27–51.
- ARNEBORG, L. 2004. Turnover times for waters above sill level in Gullmar Fjord. *Cont. Shelf Res.* **24**: 443–460.
- , AND B. LILJEBLADH. 2001. The internal seiches in Gullmar Fjord. Part II: Contribution to basin water mixing. *J. Phys. Oceanogr.* **31**: 2567–2574.
- , C. JANZEN, B. LILJEBLADH, T. P. RIPPETH, J. H. SIMPSON, AND A. STIGEBRANDT. In press. Spatial variability of diapycnal mixing and turbulent dissipation rates in a stagnant fjord basin. *J. Phys. Oceanogr.*
- AURE, J., AND R. SÆTRE. 1981. Wind effects on the Skagerrak outflow, p. 263–293. In R. Sætre and M. Mork [eds.], *The Norwegian coastal current*. Univ. Press, Bergen, Norway.
- , AND A. STIGEBRANDT. 1990. Quantitative estimates of the eutrophication effects of fish farming on fjords. *Aquaculture* **90**: 135–156.
- , J. MOLVÆR, AND A. STIGEBRANDT. 1997. Observations of inshore water exchange forced by a fluctuating offshore density field. *Mar. Pollut. Bull.* **33**: 112–119.
- BAINES, P. G. 1995. *Topographic effects in stratified flows*. Cambridge Univ. Press.
- BARINGER, M. O., AND J. F. PRICE. 1997. Mixing and spreading of the Mediterranean overflow. *J. Phys. Oceanogr.* **27**: 1654–1677.
- BJÖRK, G., AND K. NORDBERG. 2003. Upwelling along the Swedish west coast during the 20th century. *Cont. Shelf Res.* **23**: 1143–1159.
- EDWARDS, A., AND D. J. EDELSTEN. 1976. Control of fjordic deep water renewal by run-off modification. *Hydrol. Sci. Bull.* **21**: 445–450.
- GADE, H. G. 1973. Deep-water exchanges in a sill fjord. A stochastic process. *J. Phys. Oceanogr.* **3**: 213–219.
- GUSTAFSSON, B., AND A. STIGEBRANDT. 1996. Dynamics of the freshwater-influenced surface layers in the Skagerrak. *J. Sea Res.* **35**: 39–53.
- HELLE, H. B. 1978. Summer replacement of deep water in Byfjord, Western Norway: Mass exchange across the sill induced by coastal upwelling, p. 441–464. In J. C. J. Nihoul [ed.], *Hydrodynamics of estuaries and fjords*. Elsevier.
- KOUTS, T., AND A. OMSTEDT. 1993. Deep water exchange in the Baltic proper. *Tellus* **45A**: 311–324.
- LIUNGMAN, O., L. RYDBERG, AND C.-G. GÖRANSSON. 2001. Modeling and observations of deep water renewal and entrainment in a Swedish sill fjord. *J. Phys. Oceanogr.* **31**: 3401–3420.
- MOLVÆR, J. 1980. Deep-water renewals in the Frierfjord—an intermittently anoxic basin, p. 531–537. In H. J. Freeland, D. M. Farmer, and C. D. Levings [eds.], *Fjord oceanography*. Plenum.

- ÖZSOY, E., D. D. IORIO, M. C. GREGG, AND J. O. BACKHAUS. 2001. Mixing in the Bosphorus Strait and the Black Sea continental shelf: Observations and a model of the dense outflow. *J. Mar. Sys.* **31**: 99–135.
- PEDERSEN, F. B. 1980. A monograph on turbulent entrainment and friction in two-layer stratified flow. Institute of Hydrodynamics and Hydraulic Engineering Series Paper 25, Technical Univ. of Denmark.
- PETTERSSON, H. 1920. Internal movements in coastal waters and meteorological phenomena. *Geogr. Ann. Sv. Sällsk. Antropol. och Geogr.* **2**: 33–66.
- SHAFFER, G., AND L. DJURFELDT. 1983. On the low-frequency fluctuation in the eastern Skagerrak and in Gullmaren. *J. Phys. Oceanogr.* **13**: 1321–1340.
- SIMPSON, J. E. 1987. Gravity currents: In the environment and the laboratory. Ellis Horwood.
- STIGEBRANDT, A. 1977. On the effect of barotropic current fluctuations on the two-layer transport capacity of a constriction. *J. Phys. Oceanogr.* **7**: 118–122.
- . 1984. A model for the estuarine circulation in the Skagerrak, Troll field engineering studies: Oceanographic support work—Task Report 3, OTTER Report, STF88 F84017. Proprietary NHL, Trondheim.
- . 1987a. Computations of the flow of dense water into the Baltic from hydrographical measurements in the Arkona Basin. *Tellus* **39A**: 170–177.
- . 1987b. A model for the vertical circulation of the Baltic deep water. *J. Phys. Oceanogr.* **17**: 1772–1785.
- WALIN, G. 1981. On the deep water flow into the Baltic. *Geophysica* **17**: 75–93.

*Received: 20 May 2003*  
*Accepted: 26 November 2003*  
*Amended: 27 January 2004*